Published in final edited form as:
Nano Lett. 2013 March 13; 13(3): 1059–1064. doi:10.1021/nl304287a.

Lipidoid-coated Iron Oxide Nanoparticles for Efficient DNA and siRNA delivery

Shan Jiang[1,2], **Ahmed A. Eltoukhy**[1,2], **Kevin T. Love**[1,2], **Robert Langer**[1,2,3], and **Daniel G. Anderson**[1,2,3]

[1]David H Koch Institute for Integrative Cancer Research, Massachusetts Institute of Technology, 77 Massachusetts Avenue, Cambridge, MA, 02139, USA

[2]Department of Chemical Engineering, Massachusetts Institute of Technology, 77 Massachusetts Avenue, Cambridge, MA, 02139, USA

[3]Institute for Medical Engineering and Science, Massachusetts Institute of Technology, 77 Massachusetts Avenue, Cambridge, MA, 02139, USA

Abstract

The safe, targeted and effective delivery of gene therapeutics remains a significant barrier to their broad clinical application. Here we develop a magnetic nucleic acid delivery system composed of iron oxide nanoparticles and cationic lipid-like materials termed lipidoids. Coated nanoparticles are capable of delivering DNA and siRNA to cells in culture. The mean hydrodynamic size of these nanoparticles was systematically varied and optimized for delivery. While nanoparticles of different sizes showed similar siRNA delivery efficiency, nanoparticles of 50–100 nm displayed optimal DNA delivery activity. The application of an external magnetic field significantly enhanced the efficiency of nucleic acid delivery, with performance exceeding that of the commercially available lipid-based reagent, Lipofectamine 2000. The iron oxide nanoparticle delivery platform developed here offers the potential for magnetically guided targeting, as well as an opportunity to combine gene therapy with MRI imaging and magnetic hyperthermia.

Keywords

siRNA delivery; DNA delivery; iron oxide nanoparticle; magnetofection; gene therapy

Gene therapy has the potential to treat a broad range of human diseases[1]. However, the main barrier to safe and effective gene therapy remains the challenge involved in delivering these macromolecules[2]. Viral vectors have shown great efficacy of nucleic acid delivery both *in vitro* and *in vivo*, but serious safety issues continue to be a significant concern; in contrast, non-viral systems offer a number of potential advantages, including stability, low immunogenicity and toxicity[3]. Among the myriad of synthetic gene carriers that have been studied, iron oxide is an attractive material for drug delivery and theranostics for several reasons. First, iron oxide is biocompatible and biodegradable. Studies have shown that iron metabolism occurs in the human body through multiple pathways[4], and dextran-coated iron

Correspondence to: Daniel G. Anderson.

oxide nanoparticles have been clinically tested and approved by the FDA[5]. Second, the magnetic properties of iron oxide enable targeted delivery by application of an external magnetic field[6]. Third, magnetic nanoparticles can be used for MRI imaging and hyperthermia[7].

Functionalization of the iron oxide nanoparticle surface represents one of the key aspects to developing these materials as drug delivery vehicles[8]. Highly monodisperse iron oxide nanoparticles can be produced in large quantities by thermal decomposition[9], and the surfaces of these nanoparticles are most commonly coated with a layer of oleic acid or oleic amine, which can only be dispersed in a non-polar organic solvent. However, covalent conjugation of ligands to the iron oxide surface can compromise biocompatibility and degradability[8]. Silica-coated magnetic nanoparticles are water soluble and easy to functionalize, but lack biodegradability[10]. While catechol is degradable and has strong adhesion to the iron oxide nanoparticle surface, extra steps are required during modification to protect the catechol groups from oxidation[11]. Other functional groups, such as amines[12] and carboxylates[13], also have affinities for the iron oxide surface. Because this binding is non-covalent, polymers are often employed to achieve stronger adsorption[14]. To enhance stability further, these coating molecules are frequently crosslinked[15], which compromises degradability.

An alternative approach for non-covalent binding to the iron oxide surface relies on hydrophobic interaction[16]. In one method, nanoparticles and lipids are first co-precipitated and then re-dispersed in water[17]. In another method, the particles and lipids are incorporated together through an emulsion formed by an organic solvent and water, and the excess coating material was removed by magnetic separation[18]. These procedures often produce particle aggregates of heterogeneous size and lower the final yield. Furthermore, a poorly assembled lipid coating on the nanoparticle surface can detach during purification and result in the formation of unstable particle aggregates[17].

To address these challenges, we developed a simple method to coat iron oxide nanoparticles with lipids and lipid-like molecules, which produces stable nanoparticles with low polydispersity. In this method (Figure 1a), monodisperse iron oxide nanoparticles were first dispersed along with oleic acid and lipids in chloroform. Instead of completely drying the particles or forming emulsions, the solvent N-methyl-2-pyrrolidone (NMP) was added to induce adhesion between the lipids and the nanoparticle surface. Subsequently the nanoparticle and lipid mixture were sonicated under nitrogen protection. After coating the nanoparticles, chloroform was thoroughly evaporated away, which prevented phase separation when particles were transferred to the aqueous phase. Finally, the excess lipids were removed together with NMP by simply dialyzing the nanoparticles against water. Since NMP is miscible with both chloroform and water, nanoparticles remain soluble and avoid precipitation, which is undesirable due to the formation of irreversible aggregates held together by strong Van der Waals attractions[19]. Adding NMP also promotes the adhesion of the lipids to the hydrophobic nanoparticle surface in a mild manner[20], so that lipids are able to fully rearrange and assemble into a more complete layer on the nanoparticle surface[21]. As further demonstrated in Figure 1a, siRNA and DNA were then loaded onto the nanoparticle surface by electrostatic interaction with the cationic lipid coating. Once adsorbed, rather

than remain exposed at the particle surface, the siRNA and DNA molecules likely further interact with and rearrange within the lipid coating, which can consist of multiple layers. In this manner, the nucleic acids may embed within the lipid surface coating and thus be protected from enzymatic degradation.

16 nm nanoparticles were used in our experiment. An extended period of sonication was applied to keep the nanoparticles dispersed. After 5 hours of sonication, nanoparticles formed clusters after being transferred to water, as seen in Figure 1b. Continued sonication for an additional 2–3 hours resulted in the formation of individual nanoparticles, as shown in Figure 1c. A detailed transmission electron microscopy (TEM) image revealed a complete, uniform coating on the nanoparticle surface as shown in Figure 1d.

Developed with the aid of combinatorial library synthesis and screening, lipid-like materials termed lipidoids have been shown to deliver siRNA delivery both *in vitro* and *in vivo*[22]. 25 lipidoids shown in Figure S1 were synthesized and evaluated for their utility in coating iron oxide nanoparticles. The efficiencies of these formulations in delivering DNA and siRNA, respectively, to cultured HeLa cells are shown in Figure S2. Interestingly, the most effective lipidoid-coated nanoparticles for DNA delivery were also generally those that worked best for siRNA delivery. Lipidoids incorporating alkyl tails of 12 to 14 carbons in length (C12 and C14) demonstrated the best efficiencies, which is consistent with previous reports[22]. Since compound C14-200 was among the top performers in our initial *in vitro* screen for both siRNA and DNA delivery, it was selected for further study in this report. As previously described[22], additional formulation stability was conferred by initially dissolving the C14-200 lipidoid in chloroform together with 1,2-distearoyl-sn-glycero-3-phosphocholine (DSPC), cholesterol, and mPEG2000-DMG, and the ratio of these components was optimized for these experiments.

In order to test whether excess free lipids were completely purified from the nanoparticle solution, HPLC (high-performance liquid chromatography) analysis of lipid content in solution was carried out before and after the nanoparticles were extracted by means of an external magnetic field. As shown in Figure S3, most of the lipids were associated with the nanoparticles and were able to be removed by magnetically separating the nanoparticles from the solution. Measurements of siRNA concentration using the RNA binding dye RiboGreen further confirmed that the nucleic acids were associated with the positively charged nanoparticles. After magnetic extraction of the nanoparticles, little free siRNA could be detected in solution, as seen in Figure S4.

Based on the measurements of lipid and iron content of the nanoparticles after dialysis using HPLC and ICP-MS (inductively coupled plasma mass spectrometry), in a typical formulation, one nanoparticle was coated with ~1000 lipidoid molecules. For the DNA transfections, the lipid to DNA weight ratio was 1:1, with 1 DNA molecule binding to ~3 nanoparticles. For the siRNA transfections, the weight ratio of lipidoid to siRNA was 5:1, and ~100 siRNA molecules were bound onto each nanoparticle.

Both the DNA and the siRNA delivery efficiencies were tested *in vitro* using HeLa cells. DNA transfection efficiency was characterized by the percentage of GFP positive cells as

measured by fluorescence-activated cell sorting (FACS) analysis, whereas siRNA transfection efficiency was measured with a dual luciferase reporter assay used in our previous studies[22].The transfection efficiency data were plotted out together with the particle size measured by dynamic light scattering, as shown in Figure 2. In Figure 2a, as the sonication progresses, the mean hydrodynamic size of the coated nanoparticles continues to decrease from a few hundred nanometers to ~40 nm. Regardless of size, the zeta potentials for all nanoparticles were measured to be ~+20 mV in 25 mM sodium acetate buffer. Figure 2b–2c show the efficiencies of these nanoparticles for DNA and siRNA transfection, respectively. The optimal nanoparticle size for DNA delivery was 50–100 nm, for which the delivery efficiency was ~90%. For smaller-sized nanoparticles, the delivery efficiency decreased dramatically; for instance, nanoparticles of 40 nm in diameter yielded a DNA transfection efficiency of only ~ 34%. In marked contrast, siRNA transfection efficiency did not show significant variation when particles of different sizes were used, and 40 nm nanoparticles mediated highly efficient siRNA transfection corresponding to ~90% knockdown.

TEM images of DNA-loaded nanoparticles suggested a possible explanation for these observations based on the binding of DNA and siRNA molecules to the nanoparticle surface. In Figure S5, a thick amorphous layer was observed on the surface of nanoparticle clusters after mixing with DNA; however, no such structures were observed with small individual nanoparticles. The entrapment of DNA and siRNA on the nanoparticle surface as measured by a nucleic acid intercalating dye assay provided further insight[22]. As shown in Figure S6, DNA entrapment is low (<50 %) for nanoparticles smaller than 50 nm, whereas siRNA entrapment is high (~90%) and roughly uniform for all nanoparticles regardless of size.

DNA molecules have a persistence length of ~50 nm calculated by the conventional polymer random walk model[23], and free DNA molecules usually adopt a much larger size in solution. Only by interacting with certain proteins can DNA be bent into a size much smaller than its persistent length[24]. For a single 16 nm iron oxide nanoparticle, the curvature may be too high for a DNA chain to wrap tightly around it using only relatively weak electrostatic interactions, which may explain why the transfection efficiency was low when the nanoparticles were smaller than 50 nm. However, since the bending energy is inversely proportional to the square of the bending circle radius[25], bending of DNA around larger nanoparticle clusters requires much lower energies. Correspondingly, nanoparticle clusters larger than 50 nm showed much higher delivery efficiencies for DNA. On the other hand, since siRNA is a small 6 nm rod-like molecule, binding to small individual nanoparticles and large nanoparticle clusters might be equally efficient, which may account for the observation that siRNA delivery efficiency was roughly equivalent using nanoparticles of different sizes.

Application of a magnetic field directing nanoparticles towards the cell surface resulted in the enhancement of transfection efficiency (Figure 3). The left panel in Figure 3 shows the higher fluorescence intensity observed following transfection of GFP-encoding DNA in the presence of the magnetic field. Flow cytometry measurements further confirmed this observation, as shown in the right panel in Figure 3. We hypothesize that this result is due to

an increase in the physical concentration of DNA at the cell surface[26]. The dose-response profiles in Figure 4a demonstrated that the transfection efficiency remained high even at very low doses of DNA and siRNA. For DNA, a transfection efficiency of ~70% was achieved with 25 ng of DNA per well of a 96 well plate (0.05 nM). For siRNA, ~80% knockdown was achieved using 3 ng of siRNA per well (1.5 nM). In multiple experiments, using a magnet consistently increased the transfection efficiency at the lowest doses by a factor of approximately four, and the performance significantly exceeded that of the commercial transfection reagent Lipofectamine 2000. Additional experiments revealed that the transfection was accelerated as a consequence of the magnetic field, as shown in Figure 4b. For DNA delivery, in the presence of the magnet, a transfection efficiency of 50% was achieved within 4 hours of incubation at the 25 ng per well dose (0.05 nM), and quickly approached saturation after 7 hours of incubation; for siRNA,~80% knockdown was achieved within just 1 hour at the 25 ng per well dose (12.0 nM). In contrast, transfection in the absence of the magnet appeared to be much slower, and interestingly, displayed a different kinetic profile.

At a dose of 25 ng of DNA per well (0.05 nM), the viability exceeded 95%, as displayed in Figure S7. This observation is consistent with the low toxicities reported for lipidoid molecules and iron oxide nanoparticles[18, 22].Similarly, *Renilla* luciferase levels as measured by the Dual-Glo assay also indicated low cytotoxicity during siRNA transfection at the conditions tested.

In conclusion, we have developed and characterized a simple and versatile nanoparticulate DNA and siRNA delivery vehicle using lipidoids and iron oxide magnetic nanoparticles. Nanoparticles were obtained without the need for complicated synthesis and purification procedures. The method outlined here represents a broadly applicable approach for coating the surface of iron oxide nanoparticles with various lipids and lipid-like molecules. The size control attainable by this approach may make it useful for *in vivo* applications, as it has been reported that nanoparticles 50–200 nm in size are optimal for tumor targeting due to the enhanced permeability and retention (EPR) effect[27]. Furthermore, using the lipidoid-coated nanoparticles, more DNA and siRNA can be loaded onto magnetic nanoparticles as compared with direct conjugation methods[28].

Future studies will address the efficacy of these nanoparticles in mediating gene delivery to other cell types. mRNA levels can be measured to determine knockdown of other genes of interest as well as to assess changes in cellular phenotype. In addition, the incorporation of iron oxide nanoparticles imparts new functionalities to the delivery vehicle, specifically magnetic targeting, magnetic hyperthermia therapy and MRI imaging. The new delivery system may also be generalized to facilitate intracellular delivery of other negatively charged or hydrophobic drugs.

Supplementary Material

Refer to Web version on PubMed Central for supplementary material.

References

1. Verma IM, Somia N. Gene therapy - promises, problems and prospects. Nature. 1997; 389(6648): 239–242. [PubMed: 9305836]
2. Whitehead KA, Langer R, Anderson DG. Knocking down barriers: advances in siRNA delivery. Nat. Rev. Drug Discov. 2009; 8(2):129–138. [PubMed: 19180106]
3. Anderson DG, Lynn DM, Langer R. Semi-automated synthesis and screening of a large library of degradable cationic polymers for gene delivery. Angew. Chem.-Int. Edit. 2003; 42(27):3153–3158.
4. Schlachter EK, Widmer HR, Bregy A, Lonnfors-Weitzel T, Vajtai I, Corazza N, Bernau VJP, Weitzel T, Mordasini P, Slotboom J, Herrmann G, Bogni S, Hofmann H, Frenz M, Reinert M. Metabolic pathway and distribution of superparamagnetic iron oxide nanoparticles: in vivo study. Int. J. Nanomed. 2011; 6:1793–1800.
5. Tassa C, Shaw SY, Weissleder R. Dextran-Coated Iron Oxide Nanoparticles: A Versatile Platform for Targeted Molecular Imaging, Molecular Diagnostics, and Therapy. Accounts of Chemical Research. 2011; 44(10):842–852. [PubMed: 21661727]
6. Driscoll CF, Morris RM, Senyei AE, Widder KJ, Heller GS. MAGNETIC TARGETING OF MICROSPHERES IN BLOOD-FLOW. Microvasc. Res. 1984; 27(3):353–369. [PubMed: 6727704]
7. Hergt R, Dutz S, Muller R, Zeisberger M. Magnetic particle hyperthermia: nanoparticle magnetism and materials development for cancer therapy. J. Phys.-Condes. Matter. 2006; 18(38):S2919–S2934.
8. Gupta AK, Gupta M. Synthesis and surface engineering of iron oxide nanoparticles for biomedical applications. Biomaterials. 2005; 26(18):3995–4021. [PubMed: 15626447]
9. Park J, An KJ, Hwang YS, Park JG, Noh HJ, Kim JY, Park JH, Hwang NM, Hyeon T. Ultra-large-scale syntheses of monodisperse nanocrystals. Nat. Mater. 2004; 3(12):891–895. [PubMed: 15568032]
10. Kim J, Kim HS, Lee N, Kim T, Kim H, Yu T, Song IC, Moon WK, Hyeon T. Multifunctional Uniform Nanoparticles Composed of a Magnetite Nanocrystal Core and a Mesoporous Silica Shell for Magnetic Resonance and Fluorescence Imaging and for Drug Delivery. Angew. Chem.-Int. Edit. 2008; 47(44):8438–8441.
11. Amstad E, Gillich T, Bilecka I, Textor M, Reimhult E. Ultrastable Iron Oxide Nanoparticle Colloidal Suspensions Using Dispersants with Catechol-Derived Anchor Groups. Nano Letters. 2009; 9(12):4042–4048. [PubMed: 19835370]
12. El Khoury JM, Caruntu D, O'Connor CJ, Jeong KU, Cheng SZD, Hu J. Poly(allylamine) stabilized iron oxide magnetic nanoparticles. J. Nanopart. Res. 2007; 9(5):959–964.
13. Liao MH, Chen DH. Preparation and characterization of a novel magnetic nano-adsorbent. J. Mater. Chem. 2002; 12(12):3654–3659.
14. Ditsch A, Laibinis PE, Wang DIC, Hatton TA. Controlled clustering and enhanced stability of polymer-coated magnetic nanoparticles. Langmuir. 2005; 21(13):6006–6018. [PubMed: 15952854]
15. Yoon KY, Kotsmar C, Ingram DR, Huh C, Bryant SL, Milner TE, Johnston KP. Stabilization of Superparamagnetic Iron Oxide Nanoclusters in Concentrated Brine with Cross-Linked Polymer Shells. Langmuir. 2011; 27(17):10962–10969. [PubMed: 21728368]
16. Meyer EE, Lin Q, Hassenkam T, Oroudjev E, Israelachvili JN. Origin of the long-range attraction between surfactant-coated surfaces. Proceedings of the National Academy of Sciences of the United States of America. 2005; 102(19):6839–6842. [PubMed: 15863614]
17. Gonzales M, Krishnan KM. Synthesis of magnetoliposomes with monodisperse iron oxide nanocrystal cores for hyperthermia. J. Magn. Magn. Mater. 2005; 293(1):265–270.
18. Namiki Y, Namiki T, Yoshida H, Ishii Y, Tsubota A, Koido S, Nariai K, Mitsunaga M, Yanagisawa S, Kashiwagi H, Mabashi Y, Yumoto Y, Hoshina S, Fujise K, Tada N. A novel magnetic crystal-lipid nanostructure for magnetically guided in vivo gene delivery. Nature Nanotechnology. 2009; 4(9):598–606.
19. Israelachvili, JN. Intermolecular and Surface Forces. 3 ed.. Waltham, Massachusetts: Academic Press; 2010.
20. Greco FA. POLAR, APROTIC-SOLVENTS AND THE HYDROPHOBIC EFFECT. J. Phys. Chem. 1984; 88(14):3132–3133.

21. Tong S, Hou SJ, Ren BB, Zheng ZL, Bao G. Self-Assembly of Phospholipid-PEG Coating on Nanoparticles through Dual Solvent Exchange. Nano Letters. 2011; 11(9):3720–3726. [PubMed: 21793503]

22. Love KT, Mahon KP, Levins CG, Whitehead KA, Querbes W, Dorkin JR, Qin J, Cantley W, Qin LL, Racie T, Frank-Kamenetsky M, Yip KN, Alvarez R, Sah DWY, de Fougerolles A, Fitzgerald K, Koteliansky V, Akinc A, Langer R, Anderson DG. Lipid-like materials for low-dose, in vivo gene silencing. Proceedings of the National Academy of Sciences of the United States of America. 2010; 107(5):1864–1869. [PubMed: 20080679]

23. Peters JP, Maher LJ. DNA curvature and flexibility in vitro and in vivo. Q. Rev. Biophys. 2010; 43(1):23–63. [PubMed: 20478077]

24. Garcia HG, Grayson P, Han L, Inamdar M, Kondev J, Nelson PC, Phillips R, Widom J, Wiggins PA. Biological consequences of tightly bent DNA: The other life of a macromolecular celebrity. Biopolymers. 2007; 85(2):115–130. [PubMed: 17103419]

25. Boal, D. Mechanics of the Cell. 2nd ed.. Cambridge, GBR: Cambridge University Press; 2012. p. 624

26. Luo D, Saltzman WM. Enhancement of transfection by physical concentration of DNA at the cell surface. Nat. Biotechnol. 2000; 18(8):893–895. [PubMed: 10932162]

27. Maeda, H. The enhanced permeability and retention (EPR) effect in tumor vasculature: The key role of tumor-selective macromolecular drug targeting. In: Weber, G., editor. Advances in Enzyme Regulation, Vol 41. Vol. Vol. 41. Oxford: Pergamon-Elsevier Science Ltd; 2001. p. 189-207.

28. Singh N, Agrawal A, Leung AKL, Sharp PA, Bhatia SN. Effect of Nanoparticle Conjugation on Gene Silencing by RNA Interference. J. Am. Chem. Soc. 2010; 132(24):8241–8243. [PubMed: 20518524]

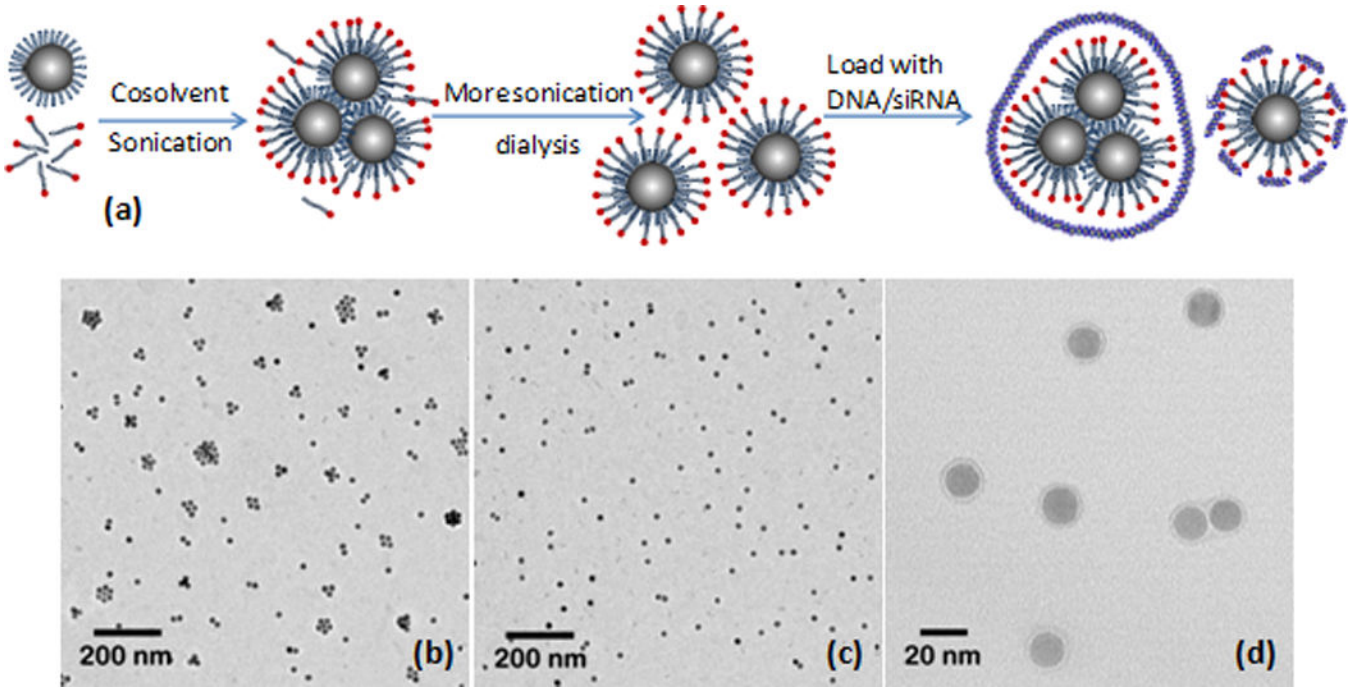

Figure 1.

(a) schematic plot of the procedure of coating iron oxide nanoparticles; transmission electron microscopy (TEM) images of (b) particle clusters; (c) individual particles; (d) coating on the nanoparticle surface.

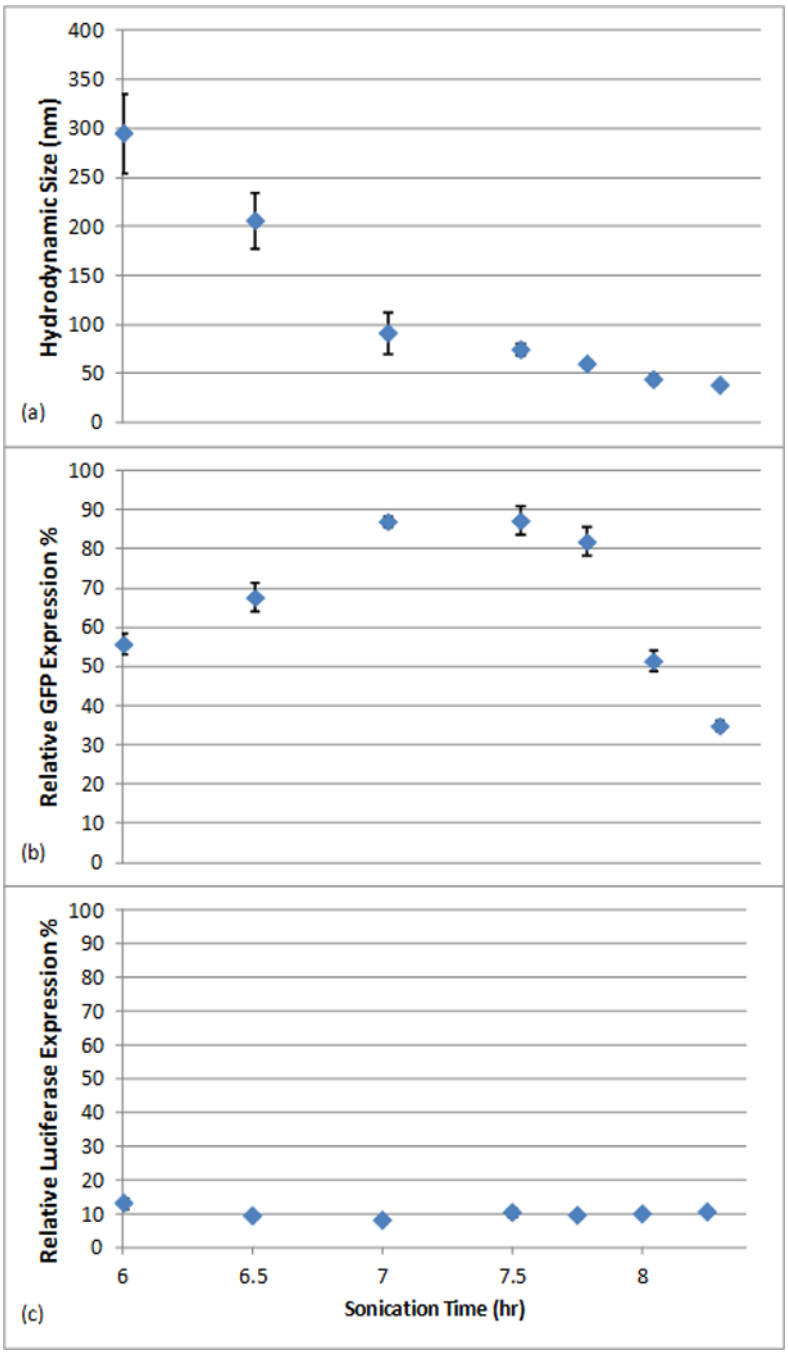

Figure 2.

(a) Particle size measured by dynamic light scattering versus sonication time; (b) DNA delivery efficiency for nanoparticles of different sizes, (25 ng of DNA per well of a 96 well plate); (c) siRNA delivery efficiency for nanoparticles of different sizes (25 ng of siRNA per well of a 96 well plate).

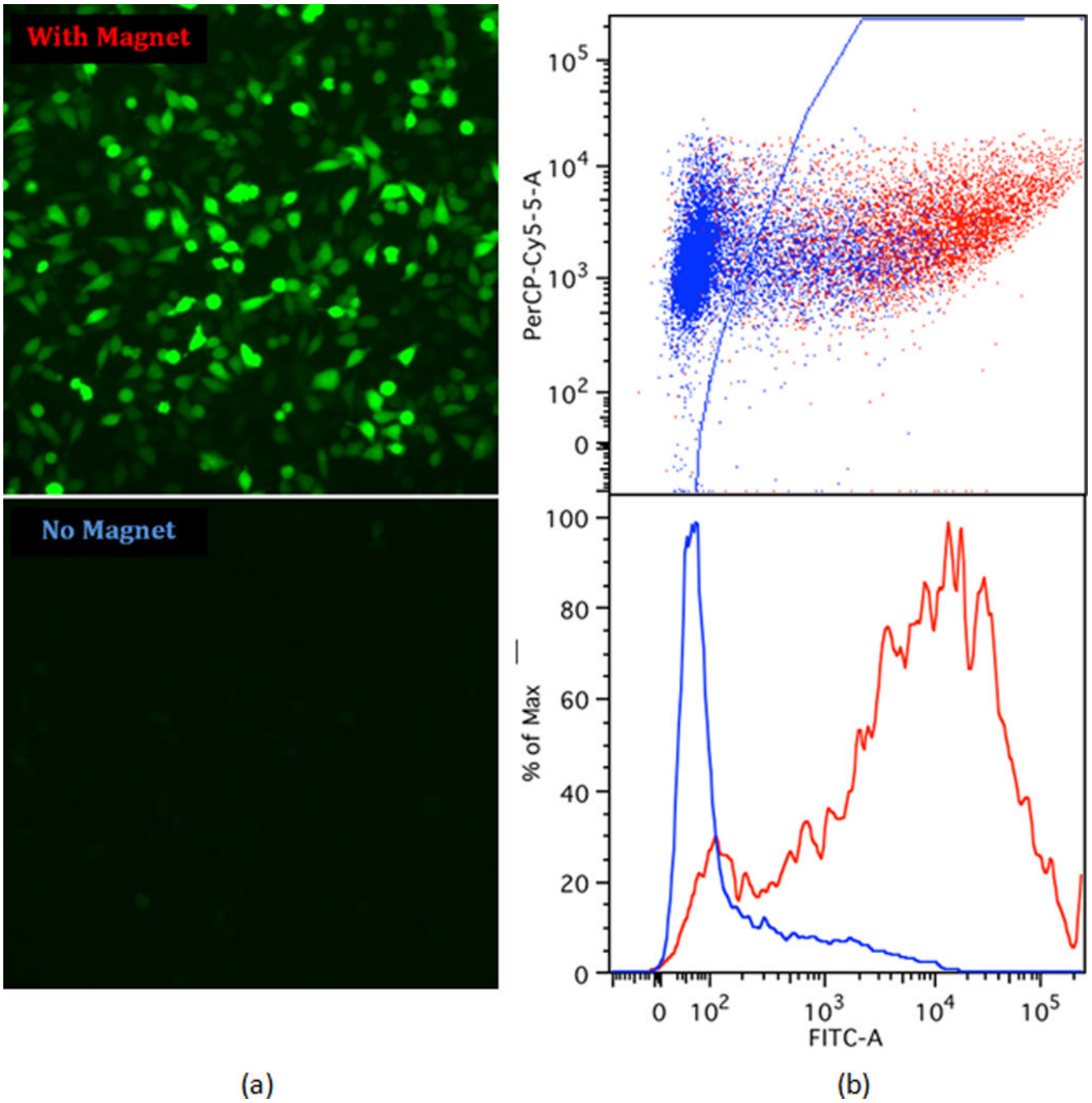

Figure 3.

Comparison of delivery efficiency with and without a magnet: (a) fluorescence microscopy images of cells after the transfection of plasmid DNA encoding green fluorescent protein (GFP) with and without the magnetic field; (b) fluorescence-activated cell sorting (FACS) analysis. Based on analysis of non-treated cells, cells to the right of the gate (blue line) were considered GFP-positive, while cells to the left of the gate were fluorescing at levels indistinguishable from background.

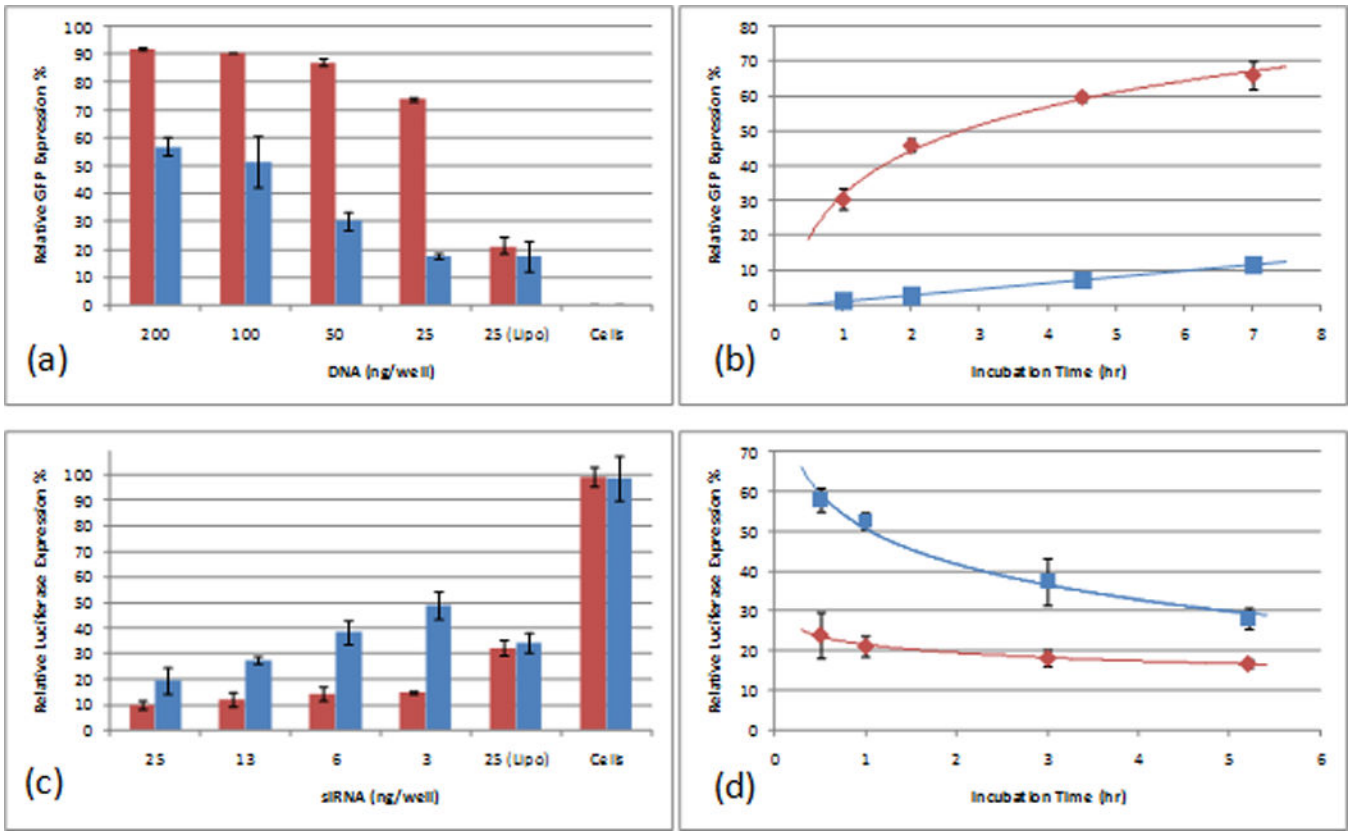

Figure 4.

Comparison of the delivery efficiency with and without a magnetic field: (a) *in vitro* DNA delivery dose response, compared with Lipofectamine2000 at 25 ng DNA per well (0.05 nM); (b) DNA delivery efficiency upon varying the incubation time; (c) siRNA delivery dose response, relative toLipofectamine2000 at 25 ng siRNA per well (12.0 nM); (d) siRNA delivery efficiency upon varying the incubation time.